Inorganic Chemistry

pubs.acs.org/IC

Article

# Disordered Crystal Structure and Anomalously High Solubility of Radium Carbonate

Artem V. Matyskin,* Burçak Ebin, Stefan Allard, Natallia Torapava, Lars Eriksson, Ingmar Persson, Paul L. Brown, and Christian Ekberg

Cite This: *Inorg. Chem.* 2023, 62, 12038−12049

Read Online

ACCESS | Metrics & More | Article Recommendations | Supporting Information

**ABSTRACT:** Radium-226 carbonate was synthesized from radium−barium sulfate ($^{226}Ra_{0.76}Ba_{0.24}SO_4$) at room temperature and characterized by X-ray powder diffraction (XRPD) and extended X-ray absorption fine structure (EXAFS) techniques. XRPD revealed that fractional crystallization occurred and that two phases were formed—the major Ra-rich phase, $Ra(Ba)CO_3$, and a minor Ba-rich phase, $Ba(Ra)CO_3$, crystallizing in the orthorhombic space group *Pnma* (no. 62) that is isostructural with witherite ($BaCO_3$) but with slightly larger unit cell dimensions. Direct-space *ab initio* modeling shows that the carbonate oxygens in the major $Ra(Ba)CO_3$ phase are highly disordered. The solubility of the synthesized major $Ra(Ba)CO_3$ phase was studied from under- and oversaturation at 25.1 °C as a function of ionic strength using NaCl as the supporting electrolyte. It was found that the decimal logarithm of the solubility product of $Ra(Ba)CO_3$ at zero ionic strength ($\log_{10} K_{sp}^0$) is −7.5(1) (2$\sigma$) ($s$ = 0.05 g·L$^{-1}$). This is significantly higher than the $\log_{10} K_{sp}^0$ of witherite of −8.56 ($s$ = 0.01 g·L$^{-1}$), supporting the disordered nature of the major $Ra(Ba)CO_3$ phase. The limited co-precipitation of $Ra^{2+}$ within witherite, the significantly higher solubility of pure $RaCO_3$ compared to witherite, and thermodynamic modeling show that the results obtained in this work for the major $Ra(Ba)CO_3$ phase are also applicable to pure $RaCO_3$. The refinement of the EXAFS data reveals that radium is coordinated by nine oxygens in a broad bond distance distribution with a mean Ra−O bond distance of 2.885(3) Å (1$\sigma$). The Ra−O bond distance gives an ionic radius of $Ra^{2+}$ in a 9-fold coordination of 1.545(6) Å (1$\sigma$).

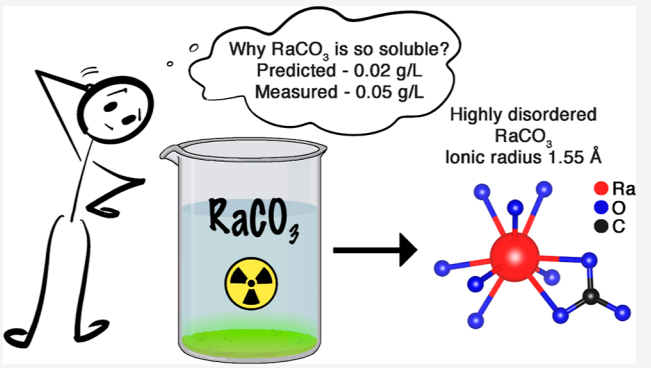


## 1. INTRODUCTION

Radium is the heaviest alkaline-earth metal and has no stable isotopes. It occurs in the earth's crust in only trace quantities (≈1 pg·g$^{-1}$)[1] as part of the $^{238}U$, $^{235}U$, and $^{232}Th$ radioactive decay series. The most long-lived and abundant radium isotope is $^{226}Ra$ with a half-life of 1600 years. Radium is among the most radiotoxic elements,[2] and if ingested, it follows similar pathways to calcium and concentrates mostly in bones and bone marrow and can cause bone sarcoma.[3] The decay chain of $^{226}Ra$ includes many alpha-, beta-, and gamma-emitting short-lived radionuclides, and dose rates even from milligram quantities of radium are significant. Moreover, $^{226}Ra$ decays to the radioactive noble gas radon, $^{222}Rn$ ($t_{1/2}$ = 3.82 days), which is also an alpha-emitter. Handling of volatile alpha emitters requires rigorous safety precautions, and as a result, experimental work even with small quantities of radium compounds is challenging, as is the case for other highly radioactive elements.[4,5]

The high radiotoxicity of radium and its decay products requires an understanding of its migration in the environment from technologically enhanced naturally occurring radioactive materials. Moreover, in 2013, a $^{223}Ra^{2+}$ ($t_{1/2}$ = 11.43 days) saline solution (trademark Xofigo©) was approved by the U.S. Food and Drug Administration and later by the European Medicines Agency for treatment of patients with castration-resistant prostate carcinomas, symptomatic bone metastases, and no known visceral metastatic disease. To date, $^{223}Ra^{2+}$ saline solution is the first and only approved radiopharmaceutical for targeted alpha therapy, but other radiopharmaceuticals with radium, for example, $CaCO_3$ microparticles radiolabeled with $^{224}Ra$ ($t_{1/2}$ = 3.63 days), are under development for local therapy of disseminated cancers and are undergoing clinical trials.[6,7]

Knowledge of the fundamental chemical properties of radium is required to understand its behavior in the environment and to exploit the therapeutic potential of radium in metastatic disease treatment. However, its chemistry

Received: May 9, 2023
Published: July 21, 2023

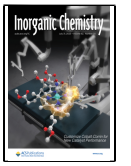

Table 1. Chemicals Used[a]

| chemical | source | purity |
|---|---|---|
| $^{226}Ra(Ba)CO_3$ powder | synthesized in house from radium sulfate[22] | mole fractions: Ra = 0.756 ± 0.010, Ba = 0.244 ± 0.006, Pb = 0.002[28] |
| $^{226}Ra$ stock solution in 2.77 mol·L$^{-1}$ HCl | synthesized in house from radium sulfate[22] using HCl from Merck (Suprapur) | mole fractions: Ra = 0.756 ± 0.005, Ba = 0.244 ± 0.003, Pb = 0.002[28] |
| $BaSO_4$ | Sigma-Aldrich | 99.998% trace metals basis |
| $Na_2CO_3$ | Sigma-Aldrich | 99.999% trace metals basis |
| NaOH | Sigma-Aldrich (Fluka) standard solution | 99.9% |
| $Na_2EDTA{\cdot}2H_2O$ | Sigma-Aldrich | 99% molecular biology grade |
| HCl | Sigma-Aldrich | 99.999% trace metals basis |
| $H_2O$ | Type 1 Merck Milli-Q | 18.2 MΩ·cm at 25 °C, total organic content <5 mg·L$^{-1}$ |
| ethanol | Solveco | Aa grade, 99.7% |

[a]Uncertainties of Ra and Ba mole fractions are 2$\sigma$ standard deviations.

remains unexplored compared with the other non-radioactive alkaline-earth metals due to the extreme rarity of radium as a laboratory material and its highly radioactive nature.[8] For example, the paper by Shannon[9] is considered one of the most comprehensive and accurate set of ionic radii; however, it includes ionic radii for radium only in 8- and 12-fold coordination but not in 9-fold. Moreover, all radium radii were estimated by Shannon[9] from plots of ionic radii ($r^3$) against unit cell volume ($V$) of isostructural series assuming that the relationship between $r^3$ and $V$ is linear. To the best of our knowledge, there are only two studies, where interatomic distances in radium compounds have been measured experimentally: Hedström and co-workers[10] studied solid radium−barium sulfate using extended X-ray absorption fine structure (EXAFS) and recently Yamaguchi et al.[11] measured diluted $HNO_3$ with 2 MBq of $^{226}Ra$ (≈4 mM) also using EXAFS. Therefore, experimental studies of radium will extend the knowledge of alkaline-earth metal chemistry applicable on both fundamental and applied levels.

Generally, it is assumed that radium chemistry is similar to that of barium due to their similar chemical and physical properties.[8] For example, radium migration in natural waters is mainly controlled by its co-precipitation with other alkaline-earth metal sulfate minerals, mostly with barite ($BaSO_4$). However, radium mobility in some natural sulfate-free waters can be controlled by its co-precipitation with various carbonate minerals, moslty with witherite ($BaCO_3$).[12] The mechanism and degree of radium co-precipitation with witherite depends mainly on crystal structures and the solubilities of pure witherite and $RaCO_3$. The crystal structure and solubility of witherite and other non-radioactive alkaline-earth metal carbonates are well established, but little is known about the properties of $RaCO_3$. Only two papers deal with the crystal structure of $RaCO_3$. It was studied experimentally by Weigel and Trinkl[13] in 1973 and by Butkalyuk and co-workers[14] in 2013. In both papers, the $RaCO_3$ samples studied were obtained by calcination (3.5 h at 640 °C and 8 h at 800 °C, respectively) and characterized using the X-ray powder diffraction (XRPD) technique. The XRPD patterns obtained are in good agreement and reveal that calcined $RaCO_3$ is isostructural with strontianite ($SrCO_3$), witherite, and cerussite ($PbCO_3$), crystallizing in the space group *Pnma* (no. 62).

To the best of our knowledge, an experimentally determined $RaCO_3$ solubility product has never been reported in the literature, although an indication that the solubility of $RaCO_3$ is significantly higher than that of witherite was first given by Nikitin[15] in 1937. Nikitin performed the following experiment: 100 mL of a solution containing 2 g of $(NH_4)_2CO_3$, 5 g of $NH_4Cl$, and 10 mL of concentrated NaOH was added to 40 mL of a pure concentrated radium solution. The formed precipitate was filtered and a mixture of HCl and $H_2SO_4$ was added to the filtrate to precipitate $RaSO_4$. Then, the mass of the precipitated $RaSO_4$ was measured. Nikitin did the same experiment with pure barium and found that the mass of precipitated $RaSO_4$ was approximately 10 times higher than the mass of precipitated $BaSO_4$, which means that the solubility product of $RaCO_3$ is approximately 10 times larger than that of $BaCO_3$ under the experimental conditions used. At that time, the theories for calculation of activity coefficients in such concentrated solutions (Specific ion Interaction Theory or Pitzer formalism) were not developed yet. Nowadays, there is evidence that $Ra^{2+}$ and $Ba^{2+}$ have similar activity coefficients in chloride and hydroxide media.[16,17] Therefore, it can be argued that the same difference (10 times) in solubilities of $BaCO_3$ and $RaCO_3$ can be expected at zero ionic strength. Moreover, recently Brown and co-workers[18] used thermodynamic modeling to derive the solubility of pure radium carbonate and showed that the decimal logarithm of the solubility product of pure radium carbonate at zero ionic strength and 25 °C is $\log_{10} K_{sp}^0 = -7.57$ ($s$ = 0.047 g·L$^{-1}$). This value is in good agreement with the experimental results obtained by Nikitin and is significantly different from the solubility product of witherite at zero ionic strength ($\log_{10} K_{sp}^0 = -8.56$).[19] This may indicate that non-calcined $RaCO_3$ is not isostructural with witherite.

Goldschmidt[20] was the first to show that radium can co-precipitate with strontianite, witherite, and cerussite in aqueous solution and determined its partition coefficients in these phases. Co-precipitation of trace radium with witherite, aragonite, calcite, and other minerals has been recently studied by other researchers[21−25] and has also been reviewed.[26,27] All reported partition (crystallization) coefficients of radium in witherite are below unity, which means that most of the radium stays in the aqueous phase and that pure $RaCO_3$ is more soluble than pure witherite. The limited co-precipitation of radium with aragonite and witherite also indicates that $RaCO_3$ may have a different crystal structure than these minerals.

However, the commonly accepted solubility product of $RaCO_3$ in the literature is from Langmuir and Riese.[12] They assumed that $RaCO_3$ is isostructural with witherite and plotted logarithms of the solubility products of strontianite, witherite, and $RaCO_3$ as functions of the effective ionic radii of $Sr^{2+}$, $Ba^{2+}$, and $Ra^{2+}$ in 8-fold coordination and estimated a $\log_{10} K_{sp}^0$ for


https://doi.org/10.1021/acs.inorgchem.3c01513
Inorg. Chem. 2023, 62, 12038−12049

$RaCO_3$ of −8.3 ($s$ = 0.02 g·$L^{-1}$) at ambient conditions and zero ionic strength.

The present study attempted to refine the crystal structure parameters of radium carbonate and gain a better understanding of the radium co-precipitation mechanism with witherite and other carbonate phases. For this purpose, a radium−barium carbonate co-precipitate was synthesized, characterized by XRPD and EXAFS techniques, and modeled using direct space methods. The solubility of $RaCO_3$ was experimentally studied as a function of ionic strength at 25.1 °C, and the apparent solubility products of $RaCO_3$ determined were extrapolated to zero ionic strength to obtain the thermodynamic value for the solubility product of $RaCO_3$.

## 2. METHODS

**Warning**: Radium sources used in this work are highly radioactive and emit the short-lived $\alpha$-emitting gas—radon. The experimental work described requires rigorous safety precautions including working in radiological fume hoods, gloveboxes, and hot cells equipped with a Rn capture system.

**2.1. Chemicals.** All experimental work with radium powder samples was performed in gloveboxes or hot cells at negative pressure and equipped with a radon capture system to avoid contamination, inhalation of radon, and ingestion of radium. All solutions were prepared using an analytical balance (Sartorius Quintix125D-1S). All chemicals used in this work are listed in Table 1.

**2.2. Synthesis of Radium Carbonate.** The initial source of radium for this work was used for brachytherapy in the 1940s to 1960s and was in the form of a steel flat plaque with five platinum-gold cylinders sealed inside the plaque. Each cylinder contained 20 mg of radium−barium sulfate powder. Disassembly of the radium source and synthesis of the radium−barium carbonate from radium−barium sulfate powder was performed as previously described[22]—the radium−barium sulfate powder was heated in 1.5 mol·$L^{-1}$ aqueous solution of $Na_2CO_3$ up to ca. 85 °C using a heating mantle. After about 90 min of heating, the solution was cooled, and the supernatant was removed. The procedure was repeated twice more. Pure $BaCO_3$ was synthesized from $BaSO_4$ using the same procedure and chemicals as used for the radium−barium carbonate synthesis. Small portions of the initial radium−barium sulfate and synthesized radium−barium carbonate were dissolved in 0.1 mol·$L^{-1}$ $Na_2EDTA$ solution and in 0.1 mol·$L^{-1}$ hydrochloric acid solution, respectively, and their purities were measured using a sector field inductively coupled plasma mass spectrometer.[28]

**2.3. XRPD and EXAFS Data Collection.** The sample for the XRPD study was prepared using a similar procedure to that previously described.[28] The whole batch of synthesized radium−barium carbonate powder was heated for 4 h at 200−250 °C using a heating mantel. After cooling, approximately 0.5 mg of radium−barium carbonate powder was placed on a low background silicon air-tight sample holder, and several drops of ethanol were added to evenly distribute the powder on the sample holder. After ethanol evaporation, the sample holder with the radium−barium carbonate powder was closed using a screw dome and transferred to another glovebox with the X-ray powder diffractometer inside. The sample holder was then placed in the measuring position, fixed in place, and the dome was removed.

The XRPD measurements of radium−barium carbonate and pure synthesized $BaCO_3$ were collected using the same procedure as described previously.[28] Both samples were approximately of the same size and were measured at 25 °C in Bragg−Brentano reflection geometry using a Bruker D2 Phaser XRPD system with Cu K$\alpha$ radiation ($\lambda$ = 1.5418 Å) equipped with a LynxEye detector. A standard reference material (NIST 640c) was measured to verify the positions of the diffraction lines and no significant deviation was found. The data were obtained by step scanning in the angle range $10° \leq 2\theta \leq 80°$ with a step increment of 0.006° ($2\theta$) and a dwell of 0.25 s per step. A 1 mm slit was used for the measurements.

For the EXAFS study, approximately 0.2 mg of the synthesized radium−barium carbonate, in the form of a number of crystals clustered together, were placed between a few Kapton tape layers and carefully sealed (sample photo is shown in the Supporting Information, Figure S1).

The EXAFS measurements of radium−barium carbonate were performed using the radium $L_3$ absorption edge. The data were collected at the wiggler beam line I811 at MAX-lab (Lund University, Sweden), which operated at 1.5 GeV and a maximum current of 180 mA. The EXAFS station was equipped with a Si[111] double-crystal monochromator for the data collection. Higher order harmonics were reduced by detuning the second monochromator crystal to reflect 70% of maximum intensity at the end of the scans. The measurement was performed in transmission and fluorescence modes simultaneously. Ten continuous scans of 10 min each were averaged. The energy calibration was performed by measuring the position of the Pb $L_2$ edge of metallic lead before and after the measurement of the radium−barium carbonate sample; the first inflection point of the Pb $L_2$ edge of metallic lead was assigned to 15,200 eV.[29]

**2.4. Solubility Data Collection.** The solubility of $RaCO_3$ was studied from under- (one sample) and oversaturation (five samples) as a function of ionic strength using NaCl (0.01, 1.3, 1.9, 2.5, 4, and 5 mol·$L^{-1}$) as a background electrolyte. For the undersaturation study, a small sample (approximately 0.5 mg), which was previously measured via XRPD, was transferred from the XRPD sample holder to the test-tube containing 0.5 mL of 0.01 mol·$L^{-1}$ NaCl. For the oversaturation studies, a previously prepared radium stock solution in the form of 2.77 mol·$L^{-1}$ HCl and with a $^{226}$Ra concentration of 0.40 ± 0.02 mmol·$L^{-1}$ was added to a solution containing $Na_2CO_3$ and NaCl. For all oversaturation samples, the sample volume was 2 mL, the concentration of $^{226}$Ra was 0.13 mmol·$L^{-1}$ and the concentration of $Na_2CO_3$ was 0.1 mol·$L^{-1}$. Preliminary experiments showed that radium sorption losses on polypropylene at such high radium concentrations were negligible. According to the literature,[30] the recommended value for the second dissociation constant ($pK_{a2}$) of $H_2CO_3$ at 25 °C and zero ionic strength is 10.239. Complete dissociation of $H_2CO_3$ in NaCl media will occur at a lower pH due to activity coefficient changes.[31] Therefore, the pH was increased by the addition of a small amount of 2 mol·$L^{-1}$ NaOH to both the under- and oversaturation samples.

All polypropylene tubes used for the solubility experiments were pre-washed first with ethanol and then with type 1 Milli-Q water to remove any residues. All samples were gently shaken under a constant temperature of 25.1 ± 0.1 °C using a shaking machine (IKA VXR basic Vibrax) coupled with a heated circulating water bath (Grant Optima T100-P12). After 39 (the undersaturation sample) and 230 (oversaturation samples) days, at least two 100 $\mu$L samples were taken and centrifuged in polypropylene tubes at 5 ·$10^4$ $g$ at a constant temperature of 25 °C for 60 min (Beckman Coulter Allegra 64R refrigerated centrifuge with F2402H rotor). The pH of all samples was measured after the last sampling and was always above 12. Radium hydrolysis at this pH is very weak and can be neglected.[16]

After centrifugation, two 10 $\mu$L samples were taken and the concentration of $^{226}$Ra was measured using a High Purity Germanium Detector (Ortec GEM-C5060 coaxial high purity germanium detector 50.5 mm diameter, 68.3 mm length, and 0.9 mm carbon epoxy entrance window coupled to a digital spectrum analyzer Ortec DSPEC50). The detector was calibrated for the same geometry (1 mL of 4 mol·$L^{-1}$ HCl in polypropylene tube) using a mixed radionuclide reference solution (NIST traceable from Eckert and Ziegler, USA). Dead time was always kept below 10%. All gamma spectra obtained were evaluated using the Gamma Vision 7.01.03 software. Radium-226 was measured using its gamma emission peak at 186.2 keV and its half-life, gamma emission energies, and photon emission probabilities were taken from the Decay Data Evaluation Project.[32]

**2.5. Data Analysis.** Refinement of the witherite and radium−barium carbonate XRPD patterns obtained was performed using the Rietveld method[33] in the Fullprof2k[34] software package, using both TREOR[35] and DICVOL-06.[36] Available witherite unit cell parame-


https://doi.org/10.1021/acs.inorgchem.3c01513
Inorg. Chem. 2023, 62, 12038−12049

ters,[37−43] corrected for the difference in ionic radius between barium and radium,[9] were used as a starting estimate.

The EXAFS oscillations were extracted from averaged raw data using standard procedures for pre-edge subtraction, spline removal, and data normalization. To obtain quantitative information for the coordination structure of the radium ion, the experimental $k^3$-weighted EXAFS oscillations were analyzed by non-linear least-squares fits of the data to the EXAFS equation, refining the model parameters: number of backscattering atoms ($N$), mean interatomic distances ($R$), Debye−Waller factor coefficients ($\sigma^2$), and threshold energy ($E_0$). Data analysis was performed using the EXAFSPAK program package.[44] Model fitting was performed with theoretical phase and amplitude functions including both single and multiple scattering paths using the *ab initio* FEFF7 code (version 7.02).[45] Diamond software[46] was used to visualize the $Ra^{2+}$ surroundings.

The apparent solubilities of $RaCO_3$ were derived as follows—first, the free $Ra^{2+}$ concentrations were calculated using values of the measured total $Ra^{2+}$ concentrations, the value of the $RaCO_3$ solubility product constant at zero ionic strength obtained from experimental data (undersaturation point at 0.01 mol·$L^{-1}$ was extrapolated to zero ionic strength using the Davies equation), and the value of the estimated stability constant of the $RaCO_3$(aq) complex at zero ionic strength taken from the literature ($\log_{10} K_0 = 2.5$).[12] The value of $RaCO_3$(aq) stability constant had a very small contribution to the calculated free $Ra^{2+}$ concentration. Then, the free $CO_3^{2-}$ concentrations were calculated using the value of the total added concentrations of $CO_3^{2-}$ and the values of the $NaCO_3^-$ stability constants. The values of the $NaCO_3^-$ stability constants were derived via non-linear curve fitting. The derived values were in good agreement with the literature values.[47−59] Subsequently, the $RaCO_3$ solubility product constants were computed as a product of the free $Ra^{2+}$ and free $CO_3^{2-}$ concentrations and then extrapolated to zero ionic strength using the extended specific ion interaction theory (ESIT). Non-linear curve fitting was performed using a Levenberg−Marquardt iteration algorithm, and the experimental apparent solubility constants of $RaCO_3$ were weighted using their standard deviations ($\omega_i = 1/\sigma^2$). Models for activity coefficients computation and adaptation of the ESIT can be found in the Supporting Information.

**2.6. Uncertainty Assessment.** The standard deviations ($2\sigma$) of the gamma spectrometric measurements of total $Ra^{2+}$ concentrations were approximately 6%. To the best of our knowledge, the stability constant of $RaCO_3$(aq) has never been measured experimentally, and therefore, the standard deviation ($2\sigma$) of the stability constant of $RaCO_3$(aq) at zero strength was estimated to be 50%. The standard deviation ($2\sigma$) of the values of the $NaCO_3^-$ stability constants were estimated based on the fitting results and an extensive literature review.[47−59] Estimation of uncertainties of stability constants of weak ion pairs including $NaCO_3^-$ is the only reliable method because in this case systematic uncertainties are much greater than stochastic.[16] The standard deviations ($2\sigma$) of the gamma spectrometric measurements, estimated $RaCO_3$(aq), and $NaCO_3^-$ stability constants were first propagated to the $2\sigma$ standard deviation of free $Ra^{2+}$ and free $CO_3^{2-}$ concentrations and then to the apparent solubility product constant of $RaCO_3$ using standard uncertainty propagation. The value for the $RaCO_3$ solubility is subject to some systematic uncertainties due to the probable presence of barium impurities. As a result, the uncertainty ($1\sigma$ standard deviation of the fit) obtained for the $RaCO_3$ solubility at zero ionic strength was increased to reflect possible systematic effects from 0.02 to 0.04 $\log_{10}$ units.

The uncertainties reported for the EXAFS refined parameters obtained are $2\sigma$ standard deviations related to the least-squares refinements. Variations in the refined parameters obtained using different models and data ranges indicate that the accuracy of the distances given for the separate complexes is within an interval of 0.005−0.02 Å, which is typical for well-defined interactions.

## 3. RESULTS

**3.1. Crystal Structure of Radium−Barium Carbonate and Its *Ab Initio* Modeling.** Rietveld refinement of the XRPD pattern of synthesized $BaCO_3$ shows that it is orthorhombic witherite and crystallizes in the *Pnma* (no. 62) space group. The unit cell parameters obtained are in good agreement with the literature values.[37−43] A comparison of the XRPD patterns of witherite and radium−barium carbonate synthesized using the same method is shown in Figure 1. As

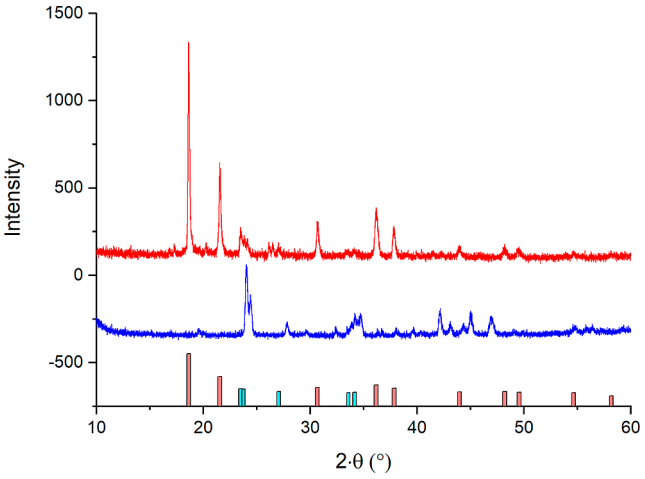


**Figure 1.** Comparison of the measured XRPD patterns of radium−barium carbonate (upper red line) and witherite (lower blue line) synthesized using the same method.

can be observed in Figure 1, the diffraction peaks in the radium−barium carbonate XRPD pattern (red) at 23.5 and 23.8° ($2\theta$) have the same shape as the diffraction peaks in the witherite XRPD pattern (blue), but they are slightly shifted to lower angles. Similar observations can be seen for the diffraction peaks in the radium−barium carbonate XRPD pattern at 27.0, 33.6, and 34.2° (Figure 1). The intensity of these diffraction peaks is much lower than the intensities of the other diffraction peaks at 18.6, 21.5, 30.7 36.2, and 37.9° (Figure 1). Thus, it can be concluded that the synthesized radium−barium carbonate contains two phases—a dominating major phase represented by ten diffraction peaks and a minor phase represented by five diffraction peaks. The small systematic shift of the five diffraction peaks in the radium−barium XRPD pattern at 23.5, 23.8, 27.0, 33.6, and 34.2° in comparison to the diffraction peaks of pure witherite shows that the minor phase is isostructural with witherite. The small systematic shift of these peaks to lower angles also shows that the minor orthorhombic $Ba(Ra)CO_3$ phase has slightly larger unit cell dimensions than witherite. This is consistent with the fact that the effective ionic radius of radium is 0.06−0.09 Å larger than that of barium, depending on the coordination number.[9] Similar differences are observed for barite and $RaSO_4$.[28]

The limited number of weak diffraction lines makes it impossible to refine any unit cell dimensions for the orthorhombic witherite-type minor phase but it can be concluded that the minor orthorhombic $Ba(Ra)CO_3$ phase is isostructural with witherite and crystallizes in the space group *Pnma* (no. 62) with slightly larger unit cell dimensions. Furthermore, it is not possible to determine precisely the barium and radium content in this minor orthorhombic phase,


https://doi.org/10.1021/acs.inorgchem.3c01513
Inorg. Chem. 2023, 62, 12038−12049

Table 2. EXAFS Refinement Parameters for the Ra $L_3$ EXAFS of the Major Ra(Ba)$CO_3$ Phase[a]

| | number of backscattering atoms | mean interatomic distance for single scattering paths, $R$ (Å) | Debye–Waller factor, $\sigma^2$ (Å$^2$) | threshold energy, $E_0$ (eV) | amplitude reduction factor, ($S_0^2$) |
|---|---|---|---|---|---|
| Ra–O | 9 | 2.885(5) | 0.0144(9) | 15,452.8(3) | 0.80(6) |
| Ra–C | 6 | 3.283(3) | 0.0090(6) | | |
| Ra–$O_{II}$ | 6 | 4.26(1) | 0.014(1) | | |
| Ra–$O_{III}$ | 12 | 4.94(4) | 0.016(2) | | |

[a]All uncertainties are 1$\sigma$ standard deviations related to the least-squares refinements.

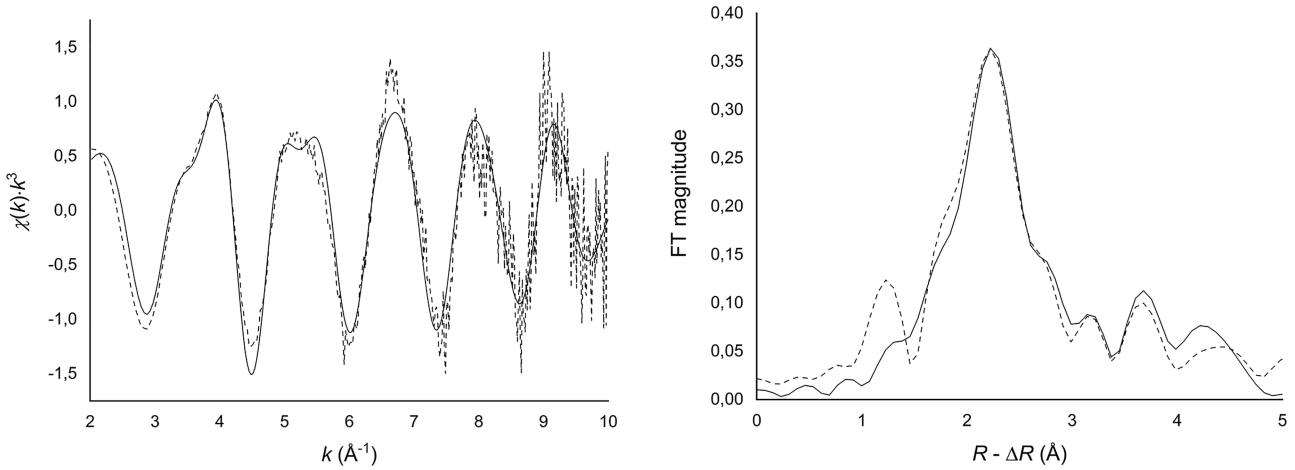


**Figure 2.** Fit (left) and Fourier transform (right) of raw EXAFS data of the major Ra(Ba)$CO_3$ phase. Dashed line—experimental and solid line—calculated.

but integration and comparison of the two most intense witherite peaks (blue) at 24.1 and 24.4° (2$\theta$) in Figure 1 with those from the radium–barium carbonate XRPD pattern (red) at 23.5 and 23.8° shows that the peak areas at 23.5, 23.8 and 24.1, 24.4° are equal to 36, 22 and 116, 59, respectively. Taking into account that sample sizes of radium–barium carbonate and pure witherite were similar and that the initial Ra/Ba molar ratio was 0.76:0.24, it can be concluded that almost all barium present in the radium–barium carbonate sample precipitated in the orthorhombic witherite phase. Moreover, the significant displacement (0.6°) of the 23.5 and 23.8° peaks and their relatively high intensity indicates that the minor witherite phase contains a significant amount of Ra. Based on the fact that the intensities of the 23.5 and 23.8° peaks from the radium–barium XRPD pattern are approximately equal to one-third of the intensities of the 24.1 and 24.4° peaks from the pure witherite XRPD pattern, it can be assumed that the approximate stoichiometry of the minor phase is $Ba_{0.7}Ra_{0.3}CO_3$ and that the major phase is almost pure radium carbonate.

The major Ra(Ba)$CO_3$ phase is represented by the high-intensity diffraction peaks at 18.6, 21.5, 30.7, 36.2, and 37.9° (Figure 1). The only two sparingly soluble metal ion carbonates in the system used in the synthesis are witherite and $RaCO_3$. The radium concentration in the initial system was significantly higher than that of barium (the Ra/Ba molar ratio was 0.76:0.24 for the mixture) and taking into account that almost all Ba precipitated in the minor orthorhombic witherite phase, it can be concluded that the major Ra(Ba)$CO_3$ phase is almost pure $RaCO_3$ with a Ba/Ra molar ratio of 0.1 or less.

The limited number of reflections did not allow for a direct Rietveld refinement of the major Ra(Ba)$CO_3$ phase structure. Attempts to solve the major Ra(Ba)$CO_3$ phase by direct space methods were made using the FOX software.[60] The model consisted of one radium atom and a carbonate ion modeled with the Avogadro software[61] and fed into FOX as a rigid molecular unit. These two objects were randomly placed and adjusted in a Monte Carlo procedure to obtain an optimal fit between the observed data and the data calculated from the present model. A dynamic occupancy correction was used for modeling the close contact and overlap of different atoms. The resulting final model showed enormous disorder features. Structural disorder in the major Ra(Ba)$CO_3$ phase results in a higher symmetry of the unit. A low symmetry cubic space group, $F23$ (no. 196), was used to not impose any additional restraints than cubic symmetry. It must be emphasized that it is hardly possible to estimate the space group with complete certainty for a sample with as few peaks as the phase investigated because of the small sample size and also the small unit cell size. However, only four formula units are required to fill the unit cell; thus, it can be modeled acceptably using the cubic $F23$ space group. Further details of the attempts to solve the crystal structure of Ra(Ba)$CO_3$ are given in the Supporting Information.

**3.2. Interatomic Distances in Radium–Barium Carbonate.** The quality of the EXAFS data for the mixture of the major Ra(Ba)$CO_3$ and minor Ba(Ra)$CO_3$ is very good despite the small amount of non-homogenized sample. Based on the XRPD pattern, it can be inferred that the derived Ra–O bond distance in the sample is dominated by the major Ra(Ba)$CO_3$ phase and that the influence of the minor Ba(Ra)$CO_3$ phase is limited. The results of the EXAFS data refinement are listed in Table 2 and the fits are shown in Figure 2.

The EXAFS data reveal a mean Ra–O bond distance of 2.885(5) Å (1$\sigma$), which indicates that radium is surrounded by


https://doi.org/10.1021/acs.inorgchem.3c01513
Inorg. Chem. 2023, 62, 12038–12049

Table 3. Comparison of Experimental, Mean Metal−Oxygen Distances in Cerussite, Strontianite, Witherite, $Ra(Ba)CO_3$, and $RaSO_4$ and Effective Ionic Radii of $Sr^{2+}$, $Pb^{2+}$, $Ba^{2+}$, and $Ra^{2+}$ in 9-fold and 12-Fold Coordination

| compound | formula | mean metal−oxygen distance[a] (Å) | metal coordination number | effective ionic radius[b] (Å) | effective ionic radius[c] (Å)[9] | references |
|---|---|---|---|---|---|---|
| cerussite | $PbCO_3$ | 2.696 | 9 | 1.356 | 1.35 | 38,39, 43, 63,−66 |
| strontianite | $SrCO_3$ | 2.645 | 9 | 1.305 | 1.31 | 38,41,43,67,−69 |
| witherite | $BaCO_3$ | 2.807 | 9 | 1.467 | 1.47 | 37−43 |
| radium carbonate | $Ra(Ba)CO_3$ | 2.885(3) | 9 | 1.545(6) | | EXAFS study, this work |
| radium nitrate solution | $Ra(NO_3)_2$ | 2.87(6) | 9.2(1.9) | 1.53(6) | | EXAFS study[11] |
| radium−barium sulfate | $Ra_{0.76}Ba_{0.24}SO_4$ | 2.96(2) | 12 | 1.62(2) | 1.7 | EXAFS study[10] |
| radium sulfate | $RaSO_4$ | 3.02 | 12 | 1.68 | 1.7 | XRPD and DFT study[28] |

[a]Calculated mean metal−oxygen bond distance from the crystal structures in the references. [b]Ionic radius of the metal ion calculated by subtracting 1.34 Å[62] from the mean metal−oxygen bond distance in the reported compounds. [c]Ionic radii proposed by Shannon.[9] Uncertainties are 1$\sigma$ standard deviations.

nine oxygen atoms from the carbonate ions in a broad bond distance distribution in solid $Ra(Ba)CO_3$. This is in good agreement with the corresponding mean metal−oxygen distances in strontianite, witherite, and cerussite, as shown in Table 3. The effective ionic radius of $Ra^{2+}$ in a 9-fold coordination can be calculated using the mean Ra−O distance from this work and an atomic radius of the carbonate oxygen of 1.34 Å from Beattie and co-workers[62] with an estimated 1$\sigma$ of 0.005 Å and compared with the effective ionic radii of $Sr^{2+}$, $Pb^{2+}$, and $Ba^{2+}$ (Table 3).

As shown in Table 3, the mean metal−oxygen distances in strontianite, witherite, cerussite, and $Ra(Ba)CO_3$ are in excellent agreement with the ionic radii for the corresponding metal ions in 9-fold coordination proposed by Shannon,[9] as well as with the atomic radius of the carbonate oxygen (1.34 Å)proposed by Beattie and co-workers.[62] Moreover, the ionic radius of $Ra^{2+}$ with the coordination number of 9(2) measured in 0.001 mol·$L^{-1}$ of $HNO_3$ via EXAFS[11] is also in good agreement with the ionic radius of $Ra^{2+}$ in 9-fold coordination measured in this work (1.53 and 1.545 Å, respectively).

The other experimental EXAFS study of a radium compound was conducted by Hedström and co-workers,[10] who studied a $RaSO_4$ sample via XRPD and EXAFS. Hedström et al.[10] assumed that the studied $RaSO_4$ sample was pure but later Matyskin et al.[28] showed that there was a barium impurity, and the actual stoichiometry of the studied sample was $Ra_{0.76}Ba_{0.24}SO_4$. EXAFS measurements give distances only between the absorbing atom (Ra) and the surrounding atoms (O), therefore the presence of the barium impurity did not affect the derived mean Ra−O bond distance.

As shown in Table 3, the mean Ra−O distance and effective ionic radius of $Ra^{2+}$ in 12-fold coordination, obtained by Hedström et al.,[10] are slightly larger, as expected, and are in good agreement with the Ra−O distance and with the effective ionic radius of $Ra^{2+}$ in 9-fold coordination obtained in this work. Later, in 2017, Matyskin et al.[28] studied the crystal structure of a radium sulfate sample of the same origin as Hedström et al.[10] also via XRPD and the derived unit cell parameters from both studies were the same. However, Matyskin et al.[28] showed that the actual stoichiometry of the studied sample was $Ra_{0.76}Ba_{0.24}SO_4$; therefore, the obtained unit cell parameters were extrapolated to the unit cell parameters of pure $RaSO_4$ using Vegard's law, and density functional theory (DFT) was used to derive the atomic coordinates and Ra−O distances in pure $RaSO_4$.[28] The derived mean Ra−O bond distance and effective ionic radius of $Ra^{2+}$ in 12-fold coordination are also in good agreement with the data obtained in this work and with the effective ionic radius estimated by Shannon[9] but is slightly larger than the data obtained by Hedström et al.[10] (Table 3). The most likely reason for the slightly shorter Ra−O bond distance derived from the EXAFS study is a possible asymmetric bond distance distribution causing the peak in the Fourier transform to be at a slightly shorter distance than the half-height center of the peak. However, the quality of the EXAFS data was not sufficient to perform detailed analysis. Moreover, the quality of the EXAFS data obtained by Hedström et al.[10] permitted only derivation of the mean Ra−O distance in $RaSO_4$, while the EXAFS data obtained in this work were of a significantly higher quality, allowing accurate extraction of longer Ra−O, Ra−C, $Ra-O_{II}$, and $Ra-O_{III}$ distances (Table 2).

The effective ionic radius of $Ra^{2+}$ in 9-fold coordination derived in this work (1.545(6) Å) is also in very good agreement with the radius of $Ra^{2+}$ in 8-fold coordination theoretically estimated by Shannon[9] (1.48 Å). Moreover, the measured mean Ra−O distance (2.885(3) Å with coordination number 9) can be compared with the Ra−O distance in the first hydration shell obtained via molecular dynamics simulations (2.93 Å with coordination number 9.8[70] and 2.85 Å with coordination number 8.1[71]).

The effective ionic radius of $Ra^{2+}$ in 9-fold coordination can be also estimated using the effective ionic radii of $Ba^{2+}$ (Figure 3). As shown in the figure, the ionic radius of $Sr^{2+}$ at each coordination number correlates very well with the corresponding ionic radius of $Ba^{2+}$ at the same coordination number (black, lower line) and this linear correlation is observed over a large range of coordination numbers (from 6 to 12). The same methodology can be applied to derive the effective ionic radius of $Ra^{2+}$ in 9-fold coordination using the available literature data for the ionic radii of $Ba^{2+}$ and $Ra^{2+}$ from Shannon[9] and the ionic radius of $Ra^{2+}$ in 6-fold coordination from Ahrens,[72] as listed by Shannon and Prewitt.[73] The correlation of $Ba^{2+}$ and $Ra^{2+}$ ionic radii result in an effective ionic radius of $Ra^{2+}$ in 9-fold coordination of 1.547 Å, which is within the 1$\sigma$ standard deviation of the value measured in this work (1.545(6) Å as listed in Table 3).

**3.3. Solubility of Radium−Barium Carbonate.** In determining the solubility, thirty-one solutions were sampled and on every occasion a few samples (3−6) were taken from the solution at each ionic strength. The activity of $^{226}Ra$ at each ionic strength was always within 10% with only one outlier.



https://doi.org/10.1021/acs.inorgchem.3c01513
Inorg. Chem. 2023, 62, 12038−12049

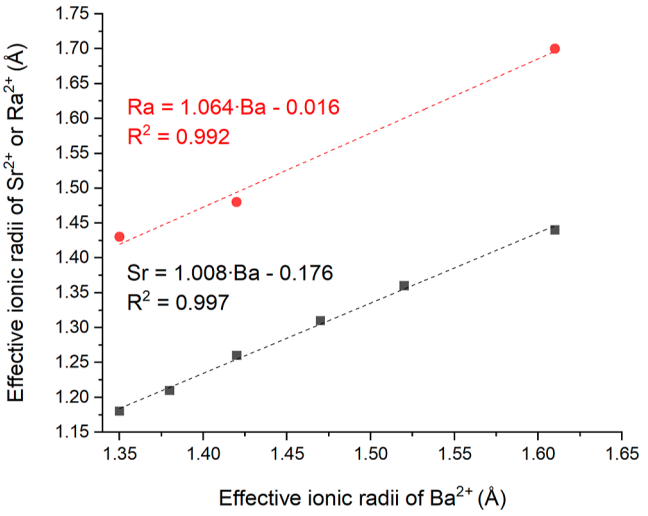


**Figure 3.** Correlation of effective ionic radii of $Ba^{2+}$ with ionic radii of $Sr^{2+}$ and $Ra^{2+}$ using the literature data.[9,72,73]

Most of the samples were centrifuged at $5{\cdot}10^4 g$, and the activity of $^{226}Ra$ was similar (within 10%) for both centrifuged and non-centrifuged samples. This indicates that $Ra(Ba)CO_3$ does not form colloids. The measured and computed concentrations of total and free $Ra^{2+}$, respectively, are listed in Table 4 (more experimental details and details about extrapolation to zero ionic strength are given in the Supporting Information).

**Table 4. Measured Total and Computed Free $Ra^{2+}$ Concentrations**[a]

| ionic strength ($mol{\cdot}kg^{-1}$) | measured concentration of total $Ra^{2+}$ ($mol{\cdot}L^{-1}$) | concentration of free $Ra^{2+}$ ($mol{\cdot}L^{-1}$) |
|---|---|---|
| 0.01 ± 0.001 | $(2.65 \pm 0.13) \times 10^{-4}$ | $(2.65 \pm 0.13) \times 10^{-4}$ |
| 1.34 ± 0.01 | $(1.19 \pm 0.06) \times 10^{-4}$ | $(1.09 \pm 0.08) \times 10^{-4}$ |
| 1.98 ± 0.01 | $(1.23 \pm 0.06) \times 10^{-4}$ | $(1.13 \pm 0.08) \times 10^{-4}$ |
| 2.65 ± 0.01 | $(1.14 \pm 0.06) \times 10^{-4}$ | $(1.05 \pm 0.08) \times 10^{-4}$ |
| 4.38 ± 0.01 | $(1.22 \pm 0.06) \times 10^{-4}$ | $(1.12 \pm 0.08) \times 10^{-4}$ |
| 5.59 ± 0.01 | $(1.19 \pm 0.12) \times 10^{-4}$ | $(1.10 \pm 0.13) \times 10^{-4}$ |

[a]All uncertainties are $2\sigma$ standard deviations. The pH of all samples was measured after the last sampling and was always above 12. The ionic strength of NaCl was recalculated from molar to molal units using the densities and relevant conversion factors.[75]

A comparison of the total and free $Ra^{2+}$ concentrations listed in Table 4 shows that the difference between the two values is less than $1{\cdot}10^{-5}$ $mol{\cdot}L^{-1}$, which means that the formation of the $RaCO_3(aq)$ complex does not significantly decrease the concentration of total $Ra^{2+}$. As also shown in Table 4, the concentrations of $Ra^{2+}$ (total and free) are within $2\sigma$ standard deviations for all ionic strengths above and equal to 1.34 $mol{\cdot}kg^{-1}$. Similar behavior is observed in the case of the solubility of aragonite ($CaCO_3$), strontianite, and witherite in NaCl media.[74]

There is ample evidence in the literature that a weak $NaCO_3^-$ ion pair is formed in aqueous media.[47−59] According to Marcus and Hefter,[76] dielectric relaxation spectroscopy has unusual capabilities for studying ion pairing phenomena. The method is particularly sensitive to very weakly associated ion pairs ($\log_{10} K^\circ < 1$) and can be used to distinguish between various types of ion pairs (solvent separated, solvent shared, and contact ion pairs). Dielectric relaxation spectroscopy was used by Capewell and co-workers[48] to determine weak $NaCO_3^-$ ion pairing in aqueous CsCl media. It was shown that the apparent stability constant of the $NaCO_3^-$ ion pair in aqueous chloride media is equal to approximately 0.3 at 1 $mol{\cdot}L^{-1}$ (i.e., $K_A \approx 0.3$) and then decreases with increasing ionic strength. The same trends and similar values for the $NaCO_3^-$ stability constants were obtained in potentiometric[49,58] and spectroscopic[56−59] studies. However, weak ion pairing is always subject to some uncertainties, mostly systematic, due to various effects: ion pair formation between components of the background medium, separation of short-range ion interaction, and weak ion pairing, among others.[16] Therefore, relatively high uncertainties were assigned to all values of the $NaCO_3^-$ stability constant obtained by numerical fitting, despite good agreement between the values obtained in this work and the literature values. The values of the apparent $NaCO_3^-$ stability constant and associated uncertainties obtained in this work and reported by Capewell and co-workers,[48] who studied $NaCO_3^-$ ion pairing by dielectric relaxation spectroscopy (also in chloride media), are listed in Table 5.

**Table 5. Stability Constants of the $NaCO_3^-$ Ion Pair from This Work and the Literature and Computed Free $CO_3^{2-}$ Concentration**[a]

| ionic strength ($mol{\cdot}kg^{-1}$) | stability constant of $NaCO_3^-$ ion pair | stability constant of $NaCO_3^-$ ion pair from Capewell et al.[48] | concentration of free $CO_3^{2-}$ ($mol{\cdot}L^{-1}$) |
|---|---|---|---|
| 1.34 ± 0.01 | 0.4 ± 0.2 | 0.3 | 0.066 ± 0.035 |
| 1.98 ± 0.01 | 0.1 ± 0.05 | 0.1 | 0.081 ± 0.034 |
| 2.65 ± 0.01 | 0.04 ± 0.02 | 0.05 | 0.091 ± 0.047 |
| 4.38 ± 0.01 | 0.002 ± 0.001 | <0.01 | 0.010 ± 0.044 |
| 5.59 ± 0.01 | 0.0003 ± 0.0002 | <0.01 | 0.010 ± 0.062 |

[a]All uncertainties are $2\sigma$ standard deviations. The pH values of all samples were measured after the last sampling and were always above 12. The ionic strength of NaCl was recalculated from molar to molal units using the densities and relevant conversion factors.[75]

As shown in Table 5, $NaCO_3^-$ ion pairing will only affect the concentration of free $CO_3^{2-}$ at the first three ionic strengths and the $NaCO_3^-$ stability constants at ionic strengths above 4 $mol{\cdot}kg^{-1}$ are too small to decrease the concentration of free $CO_3^{2-}$ in its complex formation with $Na^+$. The apparent solubility product constants of $Ra(Ba)CO_3$ were calculated as the product of the free $Ra^{2+}$ and free $CO_3^{2-}$ concentrations (Tables 4 and 5, respectively) and extrapolation of the $Ra(Ba)CO_3$ apparent solubility product constant to zero ionic strength using the ESIT is shown in Figure 4. All parameters obtained in the regression analysis are listed in Table 6.

As shown in Table 6, extrapolation of the $Ra(Ba)CO_3$ apparent solubility product constant using the Davies equation and ESIT leads to the same value for the $Ra(Ba)CO_3$ solubility product at zero ionic strength.

Millero and co-workers[74] studied the solubility of witherite in NaCl media as a function of ionic strength, and these experimental data were used to derive $\varepsilon_1$ ($Ba^{2+}$, $Cl^-$) and $\varepsilon_2$ ($Ba^{2+}$, $Cl^-$) ESIT ion interaction coefficients. The derived ESIT coefficients were used to plot the witherite solubility product as a function of NaCl ionic strength and the increase of its solubility product with an increase of the NaCl concentration is compared with that of $Ra(Ba)CO_3$ in Figure 5.


https://doi.org/10.1021/acs.inorgchem.3c01513
Inorg. Chem. 2023, 62, 12038−12049

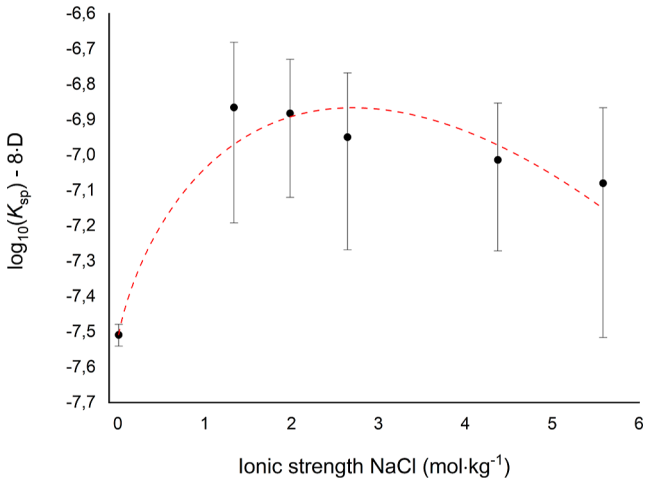


**Figure 4.** Extrapolation of experimental $\log_{10} K_{sp}$ of $Ra(Ba)CO_3$ to zero ionic strength using the ESIT. Error bars are $2\sigma$ standard deviations.

**Table 6. Solubility Product of $Ra(Ba)CO_3$ and $Ra^{2+}$−$Cl^-$ Ion Interaction Coefficients ($\varepsilon$) at 25 °C and Zero Ionic Strength**[a]

| constant | value | references |
|---|---|---|
| $\log_{10} K_{sp}^0$ of $Ra(Ba)CO_3$ | −7.52 ± 0.02 | this work—Davies equation |
| $\log_{10} K_{sp}^0$ | −7.52 ± 0.02 | this work—ESIT |
| $\varepsilon_1$ ($Ra^{2+}$, $Cl^-$) | −0.49 ± 0.05 | |
| $\varepsilon_2$ ($Ra^{2+}$, $Cl^-$) | 0.56 ± 0.07 | |

[a]All uncertainties are $1\sigma$ standard deviations.

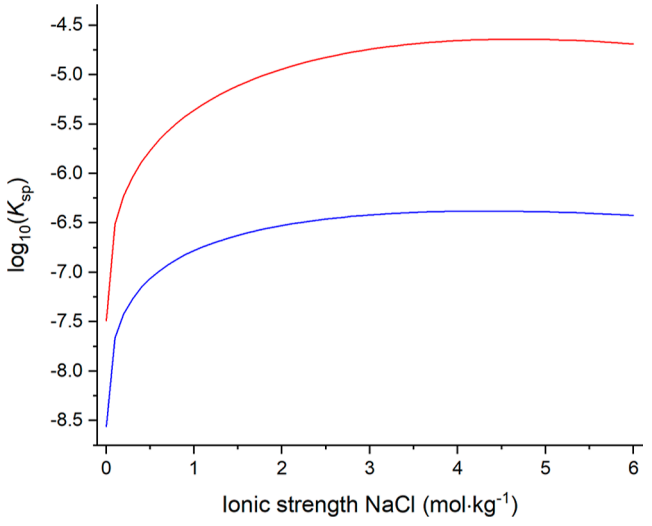


**Figure 5.** Comparison of the logarithm of the apparent $RaCO_3$ (this work) and $BaCO_3$ (witherite, from Millero et al.[74]) solubility products at different ionic strengths of aqueous NaCl media at 25 °C.

As shown in Figure 5, the shape of the solubility product curves of $Ra(Ba)CO_3$ and witherite in aqueous NaCl media are very similar, which means that $Ra^{2+}$ and $Ba^{2+}$ have similar activity coefficients and undergo similar short-range ion interactions in aqueous NaCl media. The same conclusion was obtained by Matyskin and co-workers who studied the hydrolysis of $Ra^{2+}$ and $Ba^{2+}$ in aqueous $NaClO_4$−NaOH media,[16] the complex formation of these metal ions with ethylenediaminetetraacetic acid (EDTA) also in aqueous NaCl media,[17] and the solubility product of $RaSO_4$ in aqueous NaCl media.[77]

## 4. DISCUSSION

The results obtained in the crystallographic study of this work are different to the results obtained by Weigel and Trinkl[13] and Butkalyuk and co-workers,[14] who studied $RaCO_3$ by XRPD and reported that it is isostructural with witherite. Weigel and Trinkl[13] precipitated $RaCO_3$ by addition of $(NH_4)_2CO_3$ (p.a. grade, Merck) to approximately 65 $\mu$g of $RaCl_2$ dissolved in aqueous solution (obtained from $RaBr_2$ with 98−99% purity), while Butkalyuk and co-workers[14] synthesized $RaCO_3$ by long heating of $Ra(NO_3)_2$ (with a metallic purity of 99% analyzed by inductively coupled plasma-optical emission spectroscopy) in a Ni crucible (99.99% purity). In both papers, the $RaCO_3$ sample was prepared by calcination (3.5 h at 640 °C, and 8 h at 800 °C, respectively), and the purity of the synthesized samples was not measured. In the case of $BaCO_3$ and $SrCO_3$, a phase transformation from the space group *Pnma* (orthorhombic, no. 62) to *R*3*m* (trigonal, no. 160) occurs at approximately 811[37] and 912 °C,[78] respectively, and this difference may be explained by a possible phase transformation. A similar transformation may occur for $RaCO_3$ at temperatures above 250 °C.

Another possible explanation is that the $Ra(Ba)CO_3$ co-precipitate crystallizes in a space group different from the space group of pure $RaCO_3$ or witherite due to $Ba^{2+}$ or $SO_4^{2-}$ doping. In many cases, doping can result in the formation of a compound with a crystal structure different from the crystal structure of the pure end members and can also decrease the phase transformation temperatures. An example of $SO_4^{2-}$ doping was described by Nishino and co-workers.[79] They reported that mixing witherite doped with up to 10 mol % of barite ($BaSO_4$) and heating to 820 °C for 30 min results in the formation of monoclinic $BaCO_3$ that is stable at room temperature and atmospheric pressure. However, in this work, witherite was synthesized using the same method as $Ra(Ba)CO_3$ and a typical orthorhombic witherite crystal structure was obtained. This indicates that the possible presence of small amounts of $SO_4^{2-}$ had a negligible influence on the crystal structure of the obtained $Ra(Ba)CO_3$ phase. Moreover, it can be shown that the synthesis of non-orthorhombic $BaCO_3$,[37,38,40,42] $SrCO_3$,[42] and $PbCO_3$[65,80] requires high pressures and temperatures, far above 250 °C.

An example of witherite doping with $Ca^{2+}$ and $Sr^{2+}$ has been reported in a study by Lander,[78] who synthesized barium (46 wt %), strontium (46 wt %), and calcium (8 wt %) carbonate by co-precipitation from a solution and measured the triple carbonate obtained using XRPD. Lander found that the synthesized co-precipitate was orthorhombic with a crystal structure similar to aragonite. A systematic study of the crystal structures of $Ba_{1-x}Sr_xCO_3$ co-precipitates was performed by Weinbruch and co-workers.[81] They synthesized $Ba_{1-x}Sr_xCO_3$ co-precipitates of different compositions (14 samples in total) by grinding and mixing pure witherite and strontianite and reported that all co-precipitates had orthorhombic crystal structures at room temperature. This implies that co-precipitation of $Ca^{2+}$, $Sr^{2+}$, and $Ba^{2+}$ results in the formation of stable orthorhombic phases that are isostructural with the pure end-members aragonite, strontianite, and witherite.

In summary, there is evidence in the literature that temperatures far above 250 °C are required to synthesize pure or doped $BaCO_3$ with a crystal structure different to


https://doi.org/10.1021/acs.inorgchem.3c01513
Inorg. Chem. 2023, 62, 12038−12049

witherite.[37−43] Furthermore, both methods of $Ra(Ba)CO_3$ synthesis used in the present work (three cycles of $Ra_{0.76}Ba_{0.24}SO_4$ heating in 1.5 mol·L$^{-1}$ $Na_2CO_3$ to 85 °C, cooling, and subsequent removal of the supernatant and precipitation of $Ra(Ba)CO_3$ by the addition of $RaCl_2$ solution to highly alkaline $Na_2CO_3$ solution) results in the same values of solubility product, which is approximately 10 times higher than the solubility product of witherite. This shows that the synthesis route of $Ra(Ba)CO_3$ has no influence on its solubility product or crystal structure.

The difference in the crystal structure between witherite and the major $Ra(Ba)CO_3$ phase obtained in this work can be explained by the fact that both pure $RaCO_3$ and the major $Ra(Ba)CO_3$ phase crystallize in the same space group (presumably cubic *F*-centered) with exceptional disorder. In this case, the possible barium impurity in the major $Ra(Ba)CO_3$ phase obtained would co-precipitate as a minor component and would adopt the crystal structure of pure $RaCO_3$. This hypothesis is supported by the significantly higher solubility of the major $Ra(Ba)CO_3$ phase determined in this work compared with the solubility of witherite. The decimal logarithm of the witherite solubility product at infinite dilution ($\log_{10} K_{sp}^0$) is equal to −8.56,[18] and extrapolation of this value to the solubility product of $RaCO_3$ using an electrostatic model and assuming that it is isostructural with witherite (*Pnma* no. 62) gives a value of −8.3.[12] The larger solubility product of $Ra(Ba)CO_3$ obtained in this work ($\log_{10} K_{sp}^0 = -7.5$) compared to the solubility product of witherite shows that the major $Ra(Ba)CO_3$ phase dominates and indicates that this phase is disordered because such phases usually have higher solubilities than the equivalent crystalline phases. The fact that the solubility product of $Ra(Ba)CO_3$ in NaCl media obtained from undersaturation (1 sample) and oversaturation (5 samples) is almost one order of magnitude higher than the solubility product of witherite shows that the same disordered $Ra(Ba)CO_3$ phase is systematically formed at all ionic strengths. Moreover, the solubility studies of $Ra(Ba)CO_3$ performed in this work are in a very good agreement with the findings of Nikitin,[15] who experimentally studied and compared solubilities of pure $RaCO_3$ and $BaCO_3$. Nikitin's experiments were very similar to experiments preformed in this work—he precipitated $RaCO_3$ in$NH_4Cl$ media by the addition of $(NH_4)_2CO_3$ and NaOH to $RaCl_2$ solution (total $I \approx 2.7$ mol·L$^{-1}$) and then measured the concentration of radium in the aqueous phase. The same experiments were carried out with $BaCO_3$, and it was found that the solubility of $RaCO_3$ in grams per liter was approximately 10 times higher than the solubility of $BaCO_3$ at the experimental conditions used (total $I \approx 2.7$ mol·L$^{-1}$). Thermodynamic modeling performed by Brown and co-workers,[18] who assumed that the solubility of each alkaline-earth metal carbonate is a function of the inverse of absolute temperature with a constant, but non-zero, heat capacity change, determined a solubility product for pure $RaCO_3$ of $\log_{10} K_{sp}^0 = -7.57$ ($s = 0.047$ g·L$^{-1}$). Thus, the value of the $Ra(Ba)CO_3$ solubility product determined in this work is in excellent agreement with experimental results for pure $RaCO_3$ solubility from Nikitin[15] and the thermodynamic modeling by Brown et al.[18] and the crystallographic and solubility studies of $RaCO_3$ complement each other. Additionally, according to the literature,[82] the solubility of $Ra(NO_3)_2$ is higher than the solubility of $Ba(NO_3)_2$ which is not within the trend of the solubilities of alkaline-earth metal nitrates. This indicates that a similar phenomenon may occur in $Ra(NO_3)_2$ synthesized at room temperature as was found for $RaCO_3$, and both phases have disordered oxygen atoms around the nitrogen and carbon, respectively. Another argument that $RaCO_3$ is not isostructural with witherite is the limited co-precipitation of trace $Ra^{2+}$ within witherite. To the best of our knowledge, all reported partition (crystallization) coefficients of radium in witherite are below unity,[26,27] which means that most of the radium does not co-precipitate with witherite but stays in the aqueous phase.

In summary, the following evidence confirms that the major $Ra(Ba)CO_3$ phase obtained in this work behaves as pure $RaCO_3$ and presumably crystallizes in an *F*-centered cubic space group with exceptional disorder of the carbonate ion oxygen atoms:

1. High temperatures and pressures are required to obtain pure or doped non-orthorhombic $BaCO_3$, and $BaCO_3$ synthesized using the same method as $Ra(Ba)CO_3$ always crystallizes in the orthorhombic space group.
2. The solubility product of $Ra(Ba)CO_3$ measured from both under- and oversaturation (6 measurements) shows that it is 10 times higher than witherite solubility product at zero ionic strength, and this result is consistent with literature data[15] where the solubility of pure $RaCO_3$ was measured and also with thermodynamic modeling.[18]
3. Radium co-precipitation with barium into witherite (orthorhombic $BaCO_3$) is very limited, in complete contrast to the almost complete radium co-precipitation with barium into barite (orthorhombic $BaSO_4$).
4. The effective ionic radius of $Ra^{2+}$ in 9-fold coordination determined from the EXAFS data (1.545(6) Å) is in excellent agreement with the predicted value (1.547 Å) demonstrating that the major dominant phase is almost pure $RaCO_3$.

Table 7 shows the influence of the effective ionic radii of the metal ion on the crystal structure of metal carbonates. The

**Table 7. Influence of Effective Ionic Radii of the Metal Ion on the Crystal Structure of Metal Carbonates at Ambient Conditions**

| compound | coordination number | effective ionic radii (Å)[9] | crystal system and space group |
|---|---|---|---|
| $MgCO_3$ | 6 | 0.72 | trigonal calcite type, $R\bar{3}c$ (no. 167) |
| $ZnCO_3$ | 6 | 0.74 | |
| $CoCO_3$ | 6 | 0.745 | |
| $FeCO_3$ | 6 | 0.78 | |
| $MnCO_3$ | 6 | 0.83 | |
| $CdCO_3$ | 6 | 0.95 | |
| $CaCO_3$ (calcite) | 6 | 1.0 | |
| $CaCO_3$ (aragonite) | 9 | 1.18 | orthorhombic aragonite type, *Pnma* (no. 62) |
| $SrCO_3$ | 9 | 1.31 | |
| $PbCO_3$ | 9 | 1.35 | |
| $BaCO_3$ | 9 | 1.47 | |
| $RaCO_3$ | 9 | 1.545(6)[a] | disordered, presumably *F*-centered cubic *F*23 (no. 196) |

[a]Effective ionic radius of Ra was measured in this work, and its uncertainty is 1$\sigma$ standard deviation.



https://doi.org/10.1021/acs.inorgchem.3c01513
Inorg. Chem. 2023, 62, 12038−12049

table shows that radium carbonate is the only carbonate which forms disordered crystals at ambient conditions. Possibly, the ionic radius of $Ra^{2+}$ is too large to fit into an ordered orthorhombic crystal system with carbonate ions. Moreover, the ionic radii of $Ba^{2+}$ and $Ra^{2+}$, even though close in magnitude, differ by too much to fit into their respective crystal structures, confirmed by experimental data of limited $Ba^{2+}$ co-precipitation in the major $RaCO_3$ phase and limited co-precipitation of $Ra^{2+}$ within witherite.[26,27] Differences in the crystal structure of $RaCO_3$ and witherite and limited $Ra^{2+}$ co-precipitation within witherite suggests that $Ra^{2+}$ is mostly physically absorbed during the crystal growth or at the surface of witherite.

## 5. CONCLUSIONS

In this work, a mixture of major $Ra(Ba)CO_3$ and minor orthorhombic $Ba(Ra)CO_3$ phases, dominated by the former, was synthesized at atmospheric pressure and low temperatures (below 250 °C) and measured by XRPD and EXAFS techniques. It was found that the minor orthorhombic $Ba(Ra)CO_3$ phase is isostructural with witherite and crystallizes in the space group *Pnma* (no. 62), with slightly larger unit cell dimensions due to the larger ionic radius of $Ra^{2+}$. Presumably, the major $Ra(Ba)CO_3$ phase crystallizes in the *F*-centered cubic space group with exceptional structural disorder of the carbonate ions. The derived bond distance from the EXAFS data reveals that radium is surrounded by nine oxygens from the carbonate ions in a broad bond distance distribution in solid $Ra(Ba)CO_3$ with a mean Ra−O bond distance of 2.885(3) Å. The mean Ra−O bond distance is consistent with the literature and gives an effective ionic radius of $Ra^{2+}$ in 9-fold coordination of 1.545(6) Å ($1\sigma$). The apparent solubility of $RaCO_3$ was experimentally determined as a function of ionic strength over a wide range of NaCl concentrations. It was shown that the $RaCO_3$ solubility product is one order of magnitude higher than the solubility product of witherite at all ionic strengths, which confirms that $RaCO_3$ synthesized at room temperature is not isostructural with witherite.

## ■ ASSOCIATED CONTENT

### Supporting Information

The Supporting Information is available free of charge at https://pubs.acs.org/doi/10.1021/acs.inorgchem.3c01513.

Methods used to prepare $RaCO_3$ sample for the EXAFS measurements including photo of the measured sample, details of $RaCO_3$ solubility computations including adaptation of the extended interaction theory, and results of the attempt to solve $RaCO_3$ crystal structure using Rietveld refinement combined with direct-space ab initio modeling (PDF)

## ■ AUTHOR INFORMATION


### Corresponding Author

**Artem V. Matyskin** − *Nuclear Chemistry and Industrial Materials Recycling Group, Energy and Materials Division, Department of Chemistry and Chemical Engineering, Chalmers University of Technology, SE-41296 Gothenburg, Sweden;* Present Address: Radiation Science and Engineering Center, College of Engineering, Pennsylvania State University, 135 Breazeale Nuclear Reactor, University Park, Pennsylvania, 16802, United States of America; orcid.org/0000-0002-9435-0823; Email: matyskin.artem@gmail.com

### Authors

**Burçak Ebin** − *Nuclear Chemistry and Industrial Materials Recycling Group, Energy and Materials Division, Department of Chemistry and Chemical Engineering, Chalmers University of Technology, SE-41296 Gothenburg, Sweden*

**Stefan Allard** − *Nuclear Chemistry and Industrial Materials Recycling Group, Energy and Materials Division, Department of Chemistry and Chemical Engineering, Chalmers University of Technology, SE-41296 Gothenburg, Sweden*

**Natallia Torapava** − *MAX IV Laboratory, Lund University, SE-22594 Lund, Sweden;* Present Address: Talga AB, Södra Kungsgatan 5 B, SE-972 35 Luleå, Sweden.

**Lars Eriksson** − *Arrhenius Laboratory, Department of Materials and Environmental Chemistry, Stockholm University, SE-11691 Stockholm, Sweden;* orcid.org/0000-0001-7947-3860

**Ingmar Persson** − *Department of Molecular Sciences, Swedish University of Agricultural Sciences, SE-75007 Uppsala, Sweden;* orcid.org/0000-0002-1061-7536

**Paul L. Brown** − *Rio Tinto Development and Technology, 3083 Bundoora, Victoria, Australia*

**Christian Ekberg** − *Nuclear Chemistry and Industrial Materials Recycling Group, Energy and Materials Division, Department of Chemistry and Chemical Engineering, Chalmers University of Technology, SE-41296 Gothenburg, Sweden*

Complete contact information is available at: https://pubs.acs.org/10.1021/acs.inorgchem.3c01513


### Author Contributions

A.V.M. and S.A. synthesized the samples. A.V.M., B.E., and S.A. designed the experiment and collected XRPD data. A.V.M., S.A, N.T., and I.P. designed the experiment and collected EXAFS data. A.V.M. and L.E. analyzed XRPD data. N.T. and I.P. analyzed EXAFS data. L.E. carried out direct space modeling. A.V.M. designed the experiment, collected solubility data, did $\gamma$-spectrometry, and analyzed the obtained $\gamma$-ray spectra. A.V.M., P.L.B., and C.E. analyzed solubility data. A.V.M. wrote the first manuscript draft, L.E. added direct space modeling, and N.T. and I.P. added EXAFS analysis. A.V.M., P.L.B., I.P., and C.E. finalized the manuscript. C.E. conceived the original idea for the manuscript. All authors discussed and commented on the manuscript.

### Notes

The authors declare no competing financial interest.

All data are available in the paper. Additional data and measured XRD patterns are available on request to the corresponding author.

## ■ ACKNOWLEDGMENTS

The authors are grateful to Dr. Bo Strömberg for his support. Prof. Jan John is acknowledged for his suggestions during a licentiate seminar. Dr. Rikard Ylmen, Dr. Vratislav Langer, Dr. Mark Foreman, Dr. Dmitrii Kulik, Dr. Brian L. Scott, and Dr. Mikhail Tyumentsev are acknowledged for discussions, and Mila Matyskina is acknowledged for help with graphics. This research received funding from the Swedish Radiation Protection Authority (SSM). Part of this research was carried out at beamline I811, MAX-lab synchrotron radiation source,

Lund University, Sweden. Funding for the beamline I811 project was provided by the Swedish Research Council and the Knut and Alice Wallenberg Foundation.

## REFERENCES

(1) Holmes, A. Radium and the Evolution of the Earth's Crust. *Nature* **1913**, *91*, 398.
(2) Eisenbud, M.; Gesell, T. F. *Environmental Radioactivity from Natural, Industrial & Military Sources: From Natural, Industrial and Military Sources*; Academic Press: London, 1997.
(3) Rowland, R.; Stehney, A.; Lucas, H., Jr. Dose-response relationships for female radium dial workers. *Radiat. Res.* **1978**, *76*, 368−383.
(4) Carter, K. P.; Shield, K. M.; Smith, K. F.; Jones, Z. R.; Wacker, J. N.; Arnedo-Sanchez, L.; Mattox, T. M.; Moreau, L. M.; Knope, K. E.; Kozimor, S. A.; Booth, C. H.; Abergel, R. J. Structural and spectroscopic characterization of an einsteinium complex. *Nature* **2021**, *590*, 85−88.
(5) Deblonde, G. J.-P.; Sturzbecher-Hoehne, M.; Rupert, P. B.; An, D. D.; Illy, M.-C.; Ralston, C. Y.; Brabec, J.; de Jong, W. A.; Strong, R. K.; Abergel, R. J. Chelation and stabilization of berkelium in oxidation state +IV. *Nat. Chem.* **2017**, *9*, 843−849.
(6) Westrøm, S.; Bønsdorff, T. B.; Bruland, Ø. S.; Larsen, R. H. Therapeutic Effect of $\alpha$-Emitting $^{224}$Ra-Labeled Calcium Carbonate Microparticles in Mice with Intraperitoneal Ovarian Cancer. *Transl. Oncol.* **2018**, *11*, 259−267.
(7) Westrøm, S.; Malenge, M.; Jorstad, I. S.; Napoli, E.; Bruland, Ø. S.; Bønsdorff, T. B.; Larsen, R. H. Ra-224 labeling of calcium carbonate microparticles for internal $\alpha$-therapy: Preparation, stability, and biodistribution in mice. *J. Labelled Compd. Radiopharm.* **2018**, *61*, 472−486.
(8) Brown, P. L.; Matyskin, A. V.; Ekberg, C. The aqueous chemistry of radium. *Radiochim. Acta* **2022**, *110*, 505−513.
(9) Shannon, R. D. Revised effective ionic radii and systematic studies of interatomic distances in halides and chalcogenides. *Acta Crystallogr., Sect. A: Cryst. Phys., Diffr., Theor. Gen. Crystallogr.* **1976**, *32*, 751−767.
(10) Hedström, H.; Persson, I.; Skarnemark, G.; Ekberg, C. Characterization of Radium Sulphate. *J. Nucl. Chem.* **2013**, *2013*, 1−4.
(11) Yamaguchi, A.; Nagata, K.; Kobayashi, K.; Tanaka, K.; Kobayashi, T.; Tanida, H.; Shimojo, K.; Sekiguchi, T.; Kaneta, Y.; Matsuda, S.; Yokoyama, K.; Yaita, T.; Yoshimura, T.; Okumura, M.; Takahashi, Y. Extended X-ray absorption fine structure spectroscopy measurements and ab initio molecular dynamics simulations reveal the hydration structure of the radium(II) ion. *iScience* **2022**, *25*, 104763.
(12) Langmuir, D.; Riese, A. C. The thermodynamic properties of radium. *Geochim. Cosmochim. Acta* **1985**, *49*, 1593−1601.
(13) Weigel, F.; Trinkl, A. Zur Kristallchemie des Radiums: V. Diverse Radiumsalze anorganischer Anionen. *Radiochim. Acta* **1973**, *19*, 199−202.
(14) Butkalyuk, I. L.; Butkalyuk, P. S.; Tomilin, S. V. Examination of radium compounds interaction with structural materials. *Proceedings of the Samara Russian Academy of Sciences Scientific Center*, 2013; Vol. *15* (4−5).
(15) Nikitin, B. A. Studies on the analytical chemistry of radium II. Reactions of pure radium. *Proceedings of Khlopin Radium Institute*, 1937; Vol. *3*, pp 228−237.
(16) Matyskin, A. V.; Brown, P. L.; Ekberg, C. Weak barium and radium hydrolysis using an ion exchange method and its uncertainty assessment. *J. Chem. Thermodyn.* **2019**, *128*, 362−371.
(17) Matyskin, A. V.; Hansson, N. L.; Brown, P. L.; Ekberg, C. Barium and Radium Complexation with Ethylenediaminetetraacetic Acid in Aqueous Alkaline Sodium Chloride Media. *J. Solution Chem.* **2017**, *46*, 1951−1969.
(18) Brown, P. L.; Ekberg, C.; Matyskin, A. V. On the solubility of radium and other alkaline earth sulfate and carbonate phases at elevated temperature. *Geochim. Cosmochim. Acta* **2019**, *255*, 88−104.
(19) Busenberg, E.; Plummer, L. N. The solubility of $BaCO_3$(cr) (witherite) in $CO_2$-$H_2O$ solutions between 0 and 90°C, evaluation of the association constants of $BaHCO_3^+$ (aq) and $BaCO_3^0$ (aq) between 5 and 80°C, and a preliminary evaluation of the thermodynamic properties of $Ba^{2+}$ (aq). *Geochim. Cosmochim. Acta* **1986**, *50*, 2225−2233.
(20) Goldschmidt, B. *Etude du fractionnement par cristallisation mixte à l'aide des radioéléments*; Masson et Cie, 1939.
(21) Jones, M. J.; Butchins, L. J.; Charnock, J. M.; Pattrick, R. A.; Small, J. S.; Vaughan, D. J.; Wincott, P. L.; Livens, F. R. Reactions of radium and barium with the surfaces of carbonate minerals. *Appl. Geochem.* **2011**, *26*, 1231−1238.
(22) Matyskin, A. V.; Ebin, B.; Tyumentsev, M.; Allard, S.; Skarnemark, G.; Ramebäck, H.; Ekberg, C. Disassembly of old radium sources and conversion of radium sulfate into radium carbonate for subsequent dissolution in acid. *J. Radioanal. Nucl. Chem.* **2016**, *310*, 589−595.
(23) Rihs, S.; Condomines, M.; Sigmarsson, O. U, Ra and Ba incorporation during precipitation of hydrothermal carbonates: Implications for $^{226}$Ra-Ba dating of impure travertines. *Geochim. Cosmochim. Acta* **2000**, *64*, 661−671.
(24) Yoshida, Y.; Nakazawa, T.; Yoshikawa, H. Partition coefficient of Ra in witherite. *J. Radioanal. Nucl. Chem.* **2015**, *303*, 147−152.
(25) Yoshida, Y.; Yoshikawa, H.; Nakanishi, T. Partition coefficients of Ra and Ba in calcite. *Geochem. J.* **2008**, *42*, 295−304.
(26) Curti, E. Coprecipitation of radionuclides with calcite: estimation of partition coefficients based on a review of laboratory investigations and geochemical data. *Appl. Geochem.* **1999**, *14*, 433−445.
(27) Rimstidt, J. D.; Balog, A.; Webb, J. Distribution of trace elements between carbonate minerals and aqueous solutions. *Geochim. Cosmochim. Acta* **1998**, *62*, 1851−1863.
(28) Matyskin, A. V.; Ylmen, R.; Lagerkvist, P.; Ramebäck, H.; Ekberg, C. Crystal structure of radium sulfate: An X-ray powder diffraction and density functional theory study. *J. Solid State Chem.* **2017**, *253*, 15−20.
(29) Thompson, A.; Attwood, D.; Gullikson, E.; Howells, M.; Kim, K.-J.; Kirz, J.; Kortright, J.; Lindau, I.; Liu, Y.; Pianatta, P.; Robinson, A.; Scofield, J.; Underwood, J.; Williams, G.; Winick, H. X-ray data booklet. http://xdb.lbl.gov/ (accessed 21st of January).
(30) Goldberg, R. N.; Kishore, N.; Lennen, R. M. Thermodynamic quantities for the ionization reactions of buffers. *J. Phys. Chem. Ref. Data* **2002**, *31*, 231−370.
(31) Grenthe, I.; Puigdomenech, I.; Allard, B. *Modelling in Aquatic Chemistry*; OECD Publishing, 1997.
(32) Decay Data Evaluation Project (DDEP), Laboratoire National Henri Becquerel, France. http://www.lnhb.fr/Laraweb/ Accessed on July 11, 2023.
(33) Rietveld, H. M. A profile refinement method for nuclear and magnetic structures. *J. Appl. Crystallogr.* **1969**, *2*, 65−71.
(34) Rodríguez-Carvajal, J. Recent advances in magnetic structure determination by neutron powder diffraction. *Phys. B Condens. Matter* **1993**, *192*, 55−69.
(35) Werner, P. E.; Eriksson, L.; Westdahl, M. TREOR, a semi-exhaustive trial-and-error powder indexing program for all symmetries. *J. Appl. Crystallogr.* **1985**, *18*, 367−370.
(36) Boultif, A.; Louër, D. Powder pattern indexing with the dichotomy method. *J. Appl. Crystallogr.* **2004**, *37*, 724−731.
(37) Antao, S. M.; Hassan, I. $BaCO_3$: high-temperature crystal structures and the *Pmcn*→*R3m* phase transition at 811°C. *Phys. Chem. Miner.* **2007**, *34*, 573−580.
(38) Antao, S. M.; Hassan, I. The orthorhombic structure of $CaCO_3$, $SrCO_3$, $PbCO_3$ and $BaCO_3$: linear structural trends. *Can. Mineral.* **2009**, *47*, 1245−1255.
(39) Colby, M. Y.; LaCoste, L. The crystal structure of witherite. *Z. Kristallogr.* **1935**, *90*, 1−7.


https://doi.org/10.1021/acs.inorgchem.3c01513
*Inorg. Chem.* 2023, 62, 12038−12049

(40) Holl, C.; Smyth, J.; Laustsen, H.; Jacobsen, S.; Downs, R. Compression of witherite to 8 GPa and the crystal structure of $BaCO_3$ II. *Phys. Chem. Miner.* **2000**, *27*, 467−473.
(41) De Villiers, J. P. R. Crystal structures of aragonite, strontianite, and witherite. *Am. Mineral.* **1971**, *56*, 758−767.
(42) Strømme, K.; George, J. W.; Husebye, S.; Mikalsen, Ø.; Southern, J. T.; Edlund, K.; Eliasen, M.; Herskind, C.; Laursen, T.; Pedersen, P. M. On the Crystal Structures of the High-temperature Forms of Strontium and Barium Carbonate and Structurally Related Compounds. *Acta Chem. Scand., Ser. A* **1975**, *29a*, 105−110.
(43) Ye, Y.; Smyth, J. R.; Boni, P. Crystal structure and thermal expansion of aragonite-group carbonates by single-crystal X-ray diffraction. *Am. Mineral.* **2012**, *97*, 707−712.
(44) George, G. N.; Pickering, I. J. *EXAFSPAK: A Suite of Computer Programs for Analysis of X-ray Absorption Spectra*; SSRL: Stanford, 1993.
(45) Zabinsky, S. I.; Rehr, J. J.; Ankudinov, A.; Albers, R. C.; Eller, M. J. Multiple-scattering calculations of x-ray-absorption spectra. *Phys. Rev. B* **1995**, *52*, 2995−3009.
(46) Brandenburg, K.; Putz, H. DIAMOND—crystal and molecular structure visualization. http://www.crystalimpact.com/diamond (accessed January 26, 2023).
(47) Butler, J. N.; Huston, R. Activity coefficients and ion pairs in the systems sodium chloride-sodium bicarbonate-water and sodium chloride-sodium carbonate-water. *J. Phys. Chem.* **1970**, *74*, 2976−2983.
(48) Capewell, S.; Buchner, R.; Hefter, G.; May, P. Dielectric relaxation of aqueous $Na_2CO_3$ solutions. *Phys. Chem. Chem. Phys.* **1999**, *1*, 1933−1937.
(49) Capewell, S. G.; Hefter, G.; May, P. M. Potentiometric Investigation of the Weak Association of Sodium and Carbonate Ions at 25°C. *J. Solution Chem.* **1998**, *27*, 865−877.
(50) Crea, F.; Stefano, C. D.; Gianguzza, A.; Piazzese, D.; Sammartano, S. Protonation of carbonate in aqueous tetraalkylammonium salts at 25°C. *Talanta* **2006**, *68*, 1102−1112.
(51) Daniele, P. G.; Foti, C.; Gianguzza, A.; Prenesti, E.; Sammartano, S. Weak alkali and alkaline earth metal complexes of low molecular weight ligands in aqueous solution. *Coord. Chem. Rev.* **2008**, *252*, 1093−1107.
(52) Garrels, R. M.; Thompson, M. E. A chemical model for sea water at 25 degrees C and one atmosphere total pressure. *Am. J. Sci.* **1962**, *260*, 57−66.
(53) Garrels, R. M.; Thompson, M. E.; Siever, R. Control of carbonate solubility by carbonate complexes. *Am. J. Sci.* **1961**, *259*, 24−45.
(54) Mojica Prieto, F. J.; Millero, F. J. The values of $pK_1 + pK_2$ for the dissociation of carbonic acid in seawater. *Geochim. Cosmochim. Acta* **2002**, *66*, 2529−2540.
(55) Pytkowicz, R. M.; Hawley, J. E. Bicarbonate and carbonate ion-pairs and a model of seawater at 25°C. *Limnol. Oceanogr.* **1974**, *19*, 223−234.
(56) Schmidt, C. Raman spectroscopic determination of carbon speciation and quartz solubility in $H_2O$+$Na_2CO_3$ and $H_2O$+$NaHCO_3$ fluids to 600 °C and 1.53 GPa. *Geochim. Cosmochim. Acta* **2014**, *145*, 281−296.
(57) Sipos, P.; Bolden, L.; Hefter, G.; May, P. M. Raman Spectroscopic Study of Ion Pairing of Alkali Metal Ions with Carbonate and Sulfate in Aqueous Solutions. *Aust. J. Chem.* **2000**, *53*, 887−890.
(58) Stefánsson, A.; Bénézeth, P.; Schott, J. Carbonic acid ionization and the stability of sodium bicarbonate and carbonate ion pairs to 200°C − A potentiometric and spectrophotometric study. *Geochim. Cosmochim. Acta* **2013**, *120*, 600−611.
(59) Wu, J.; Wang, S.; Zheng, H. The influence of ionic strength on carbonate-based spectroscopic barometry for aqueous fluids: an in-situ Raman study on $Na_2CO_3$-NaCl solutions. *Sci. Rep.* **2016**, *6*, 39088.
(60) Favre-Nicolin, V.; Černý, R. *FOX*, 'free objects for crystallography': a modular approach to *ab initio* structure determination from powder diffraction. *J. Appl. Crystallogr.* **2002**, *35*, 734−743.
(61) Hanwell, M. D.; Curtis, D. E.; Lonie, D. C.; Vandermeersch, T.; Zurek, E.; Hutchison, G. R. Avogadro: an advanced semantic chemical editor, visualization, and analysis platform. *J. Cheminf.* **2012**, *4*, 17.
(62) Beattie, J. K.; Best, S. P.; Skelton, B. W.; White, A. H. Structural studies on the caesium alums, $CsM^{III}[SO_4]_2{\cdot}12H_2O$. *J. Chem. Soc., Dalton Trans.* **1981**, 2105−2111.
(63) Zemann, J.; Wildner, M.; Jarosch, D.; Heger, G.; Giester, G.; Chevrier, G. Neutron single-crystal refinement of cerussite, $PbCO_3$, and comparison with other aragonite-type carbonates. *Z. Kristallogr.* **1992**, *199*, 67−74.
(64) Gordon, L.; Rowley, K. Coprecipitation of radium with barium sulfate. *Anal. Chem.* **1957**, *29*, 34−37.
(65) Minch, R.; Peters, L.; Ehm, L.; Knorr, K.; Siidra, O. I.; Prakapenka, V.; Dera, P.; Depmeier, W. Evidence for the existence of a $PbCO_3$-II phase from high pressure X-ray measurements. *Z. Kristallogr.* **2010**, *225*, 146−152.
(66) Sahl, K. Verfeinerung der kristallstruktur von cerussit, $PbCO_3$. *Z. Kristallogr.* **1974**, *139*, 215−222.
(67) Jarosch, D.; Heger, G. Neutron diffraction investigation of strontianite, $SrCO_3$. *Bull. Minéral.* **1988**, *111*, 139−142.
(68) Pannhorst, W.; Löhn, J. Zur kristallstruktur von strontianit, $SrCO_3$. *Z. Kristallogr.* **1970**, *131*, 455−459.
(69) Zachariasen, W. H., *Untersuchungen über die Kristallstruktur von Sesquioxyden und Verbindungen ABO−3, von William Houlder Zachariasen*; i kommisjon HJ Dybwad: 1928; p 165.
(70) Pappalardo, R. R.; Caralampio, D. Z.; Martínez, J. M.; Sánchez Marcos, E. Hydration of Heavy Alkaline-Earth Cations Studied by Molecular Dynamics Simulations and X-ray Absorption Spectroscopy. *Inorg. Chem.* **2021**, *60*, 13578−13587.
(71) Matsuda, A.; Mori, H. Theoretical Study on the Hydration Structure of Divalent Radium Ion Using Fragment Molecular Orbital−Molecular Dynamics (FMO−MD) Simulation. *J. Solution Chem.* **2014**, *43*, 1669−1675.
(72) Ahrens, L. H. The use of ionization potentials Part 1. Ionic radii of the elements. *Geochim. Cosmochim. Acta* **1952**, *2*, 155−169.
(73) Shannon, R. D.; Prewitt, C. T. Effective ionic radii in oxides and fluorides. *Acta Crystallogr., Sect. B: Struct. Sci., Cryst. Eng. Mater.* **1969**, *25*, 925−946.
(74) Millero, F. J.; Milne, P. J.; Thurmond, V. L. The solubility of calcite, strontianite and witherite in NaCl solutions at 25°C. *Geochim. Cosmochim. Acta* **1984**, *48*, 1141−1143.
(75) Silva, R. J.; Bidoglio, G.; Robouch, P.; Puigdomènech, I.; Wanner, H.; Rand, M. *Chemical Thermodynamics of Americium*; Newnes, 2012; Vol. *2*.
(76) Marcus, Y.; Hefter, G. Ion Pairing. *Chem. Rev.* **2006**, *106*, 4585−4621.
(77) Matyskin, A. V. *Solubility and Crystal Structure of Radium Sulfate and Carbonate*; Chalmers University of Technology: Gothenburg, 2019.
(78) Lander, J. Polymorphism and anion rotational disorder in the alkaline earth carbonates. *J. Chem. Phys.* **1949**, *17*, 892−901.
(79) Nishino, T.; Sakurai, T.; Ishizawa, N.; Mizutani, N.; Kato, M. Characterization of a new $SO_4^{2-}$ - stabilized phase of $BaCO_3$. *J. Solid State Chem.* **1987**, *69*, 24−29.
(80) Catalli, K.; Santillan, J.; Williams, Q. A high pressure infrared spectroscopic study of $PbCO_3$-cerussite: constraints on the structure of the post-aragonite phase. *Phys. Chem. Miner.* **2005**, *32*, 412−417.
(81) Weinbruch, S.; Büttner, H.; Rosenhauer, M. The ortho-rhombic-hexagonal phase transformation in the system $BaCO_3$-$SrCO_3$ to pressures of 7000 bar. *Phys. Chem. Miner.* **1992**, *19*, 289−297.
(82) Erbacher, O. Löslichkeits-Bestimmungen einiger Radiumsalze. *Ber. Dtsch. Chem. Ges.* **1930**, *63*, 141−156.


https://doi.org/10.1021/acs.inorgchem.3c01513
*Inorg. Chem.* 2023, 62, 12038−12049